Sacrificing Adaptability for Functionality: The Ivory Tower of Macular Müller Cells

Ting Zhang[#1], Kaiyu Jin[#2], Shaoxue Zeng[1], Penghui Yang[2], Meidong Zhu[3], Jialing Zhang[1], Yingying Chen[1,4], Sora Lee[1], Michelle Yam[1], Yue Zeng[1,4], Xiaoyan Lu[2], Lipin Loo[5], G. Gregory Neely[5], Andrew Chang[6], Fanfan Zhou[7], Jianhai Du[8], Xiaohui Fan[*2,9], Ling Zhu[*1], Mark C. Gillies[1]

1. Macula Research Group, Save Sight Institute, Faculty of Medicine and Health, The University of Sydney, Sydney, NSW 2006, Australia.

2. Pharmaceutical Informatics Institute, College of Pharmaceutical Sciences, Zhejiang University, Hangzhou, Zhejiang 310058, China.

3. New South Wales Tissue Bank, New South Wales Organ and Tissue Donation Service, Sydney, NSW, 2000, Australia.

4. Department of Ophthalmology, West China Hospital, Sichuan University, Chengdu, Sichuan 610041, China.

5. Charles Perkins Centre, Dr. John and Anne Chong Lab for Functional Genomics, Centenary Institute and School of Life and Environmental Sciences, University of Sydney, Camperdown, New South Wales, Australia

6. Save Sight Institute, Faculty of Medicine and Health, The University of Sydney, Sydney, NSW, 2000, Australia

7. Molecular Drug Development Group, Sydney Pharmacy School, Faculty of Medicine and Health, The University of Sydney, Sydney, NSW 2006, Australia.

8. Departments of Ophthalmology and Visual Sciences and Biochemistry and Molecular Medicine, West Virginia University, Morgantown, WV, 26506, United States.

9. National Key Laboratory of Chinese Medicine Modernization, Innovation Centre of Yangtze River Delta, Zhejiang University, Jiaxing 314103, China.

# equal contribution first authors

* co-corresponding authors

Abstract

The predilection of many conditions, such as macular telangiectasia type 2, for the human macula suggests it may be more susceptible to stress than the peripheral retina. In this study, we have comprehensively investigated the transcriptomic profiling of the macula and peripheral retina in response to stress. We conducted single-cell RNA sequencing analysis on the macula and peripheral retina of four donors cultured ex vivo with or without exposure to light stress. We found that the peripheral retina generally exhibited more transcriptional changes than the macula in response to stress. Interestingly, one of the most pronounced changes was observed in a subgroup of Müller cells that are dominant in the peripheral retina. Genes more abundantly expressed in peripheral retinal Müller cells were mainly associated with stress responses and were more influenced by light stress. In contrast, genes that were highly expressed in Müller cells that predominate in the macula played roles in cellular function and were less influenced by light stress. We identified that Metallothionein 1 (MT1), A Kinase Anchor Protein 12 (AKAP12) and MAF BZIP Transcription Factor F (MAFF) were more abundantly expressed in peripheral Müller cells than in macular Müller cells. We found that these genes were also activated in the mouse retina in the early stages of development of subretinal neovascularisation. Knockdown of the MT1, AKAP12 and MAFF genes in human primary Müller cells reduced cell viability in response to light stress and disrupted several stress response pathways. Taken together, our findings indicate that macular Müller cells are more directed toward maintaining retinal cell function rather than mounting a stress response when they are exposed to acute stress, which may contribute to the macula's vulnerability to degenerative disease.

Introduction

The neurosensory retina is a remarkable tissue that converts light stimuli into neurochemical signals transmitted to the brain for visual perception. The retina comprises diverse cell types, including photoreceptors, horizontal cells, bipolar cells, amacrine cells, retinal ganglion cells and Müller cells. It is a complex network where these neurons and glial cells interact closely to maintain retinal structure and homeostasis, ensuring optimal visual function.

The macula, a specialised cone-rich region located at the centre of the retina, is responsible for colour and high-acuity central vision. This functionally important area is more prone than the peripheral retina to develop many diseases, such as age-related macular degeneration (AMD), diabetic macular edema (DME) and Macular telangiectasia type 2 (MacTel) [1, 2] for reasons that remain largely unknown. It has been hypothesised that it may primarily be due to the complex molecular interactions among the diverse retinal cell types and the multifactorial nature of the underlying pathological processes [3]. We hypothesise that the macula is more prone to developing disease than the peripheral retina because it is less able to mount an effective response against stress.

Müller cells, the principal glial cells of the retina, span the entire thickness of the vertebrate neural retina. They play a crucial role in maintaining the structural and functional stability of the retina, which is densely populated with various cell types. Müller cells are specifically involved in regulating transcellular ion and water transport, maintaining the blood-retinal barrier and modulating neurotransmitter levels [4]. Additionally, they supply trophic factors, metabolites and antioxidants to photoreceptors and neurons, store glycogen and facilitate light transmission to photoreceptors. Müller cells also can regenerate neurons and photoreceptors in response to stress or injury [5]. We have previously reported that macula- and periphery-dominant primary Müller cells exhibit distinct transcriptomic profiles, as evidenced by bulk RNA sequencing results [6]. However, how this correlates with their distinctive responses to stress is yet to be clarified.

Light exposure induces age-related and oxidative stress in the retina through various mechanisms, including generating reactive oxygen species (ROS), chronic inflammation, photoreceptor damage and compromised cellular repair mechanisms [7-9]. Light-stressed retinas in laboratory animals have been widely used in the study of retinal degeneration [9, 10]. In this study, we compared the single-cell transcriptomic profiles of human retinal explants from both the macula and peripheral retina exposed to high-intensity or dim light. We hoped to gain insights into the reasons underlying the macula's particular vulnerability to developing degenerative disease.

Results

Identification of human retinal cell types in the *ex vivo* cultured macula and peripheral retinas

We conducted a transcriptional analysis of 16 retinal explants from 4 *postmortem* human donor eyes **(Supplementary Table 1)**, comprising paired macular and peripheral retinas with and without light stress. The macular and mid-peripheral neural retinas from the left eyes were exposed to intense light (32K lux) for 4 hours, while the corresponding regions from the right eyes were subjected to dim light (5 lux) as controls (**Supplementary Figure 2**). We then investigate gene expression at the single-cell level (**Figure 1A)**.

We obtained 77,405 transcriptomic profiles, including 19,419 profiles from the Peripheral retinas with Light stress (LP), 19,887 profiles from the Peripheral retinas with dim light as the Control (CP), 18,290 profiles from the Macula with Light stress (LM) and 19,809 profiles from the macula with dim light as the Control (CM). The sequencing depth (indicated by the average unique genes detected per cell) is illustrated in **Supplementary Figure 3A**. Overall gene expression patterns were very similar across the 4 donors (**Supplementary Figure 3B**).

We employed unsupervised clustering, uniform manifold approximation and projection (UMAP) dimensionality reduction techniques to analyse the integrated dataset. Based on the

expression of established, retinal cell-specific markers, we identified 10 major retinal cell populations (**Figure 1B** and **Supplementary Figure 3C**). Each cell population was characterised by a set of unique signature genes (**Figure 1C**): rods (42,687 cells), cones (1573 cells), bipolar cells (11,530 cells), retinal ganglion cells (2,281 cells), amacrine cells (1,071 cells), horizontal cells (965 cells), Müller cells (15,430 cells), astrocytes (943 cells), microglia (814 cells) and vascular endothelial cells (111 cells).

The cellular composition of the macula and peripheral retina were significantly different (**Figure 1D**): Retinal ganglion cells (5.87% vs. 0.11%), cones (2.32% vs. 1.75%) and rods (44.5% vs. 65.5%). We also examined the distribution and expression pattern of the cell populations across the 4 treatment groups (LP, CP, LM and CM) (**Supplementary Figure 3D**). The proportions of cell populations in the macula and peripheral retinas did not differ between the groups exposed to bright or dim light. The degree of transcriptomic changes caused by light stress was not as great as the differences between the macula and peripheral retina (**Figure 1E**).

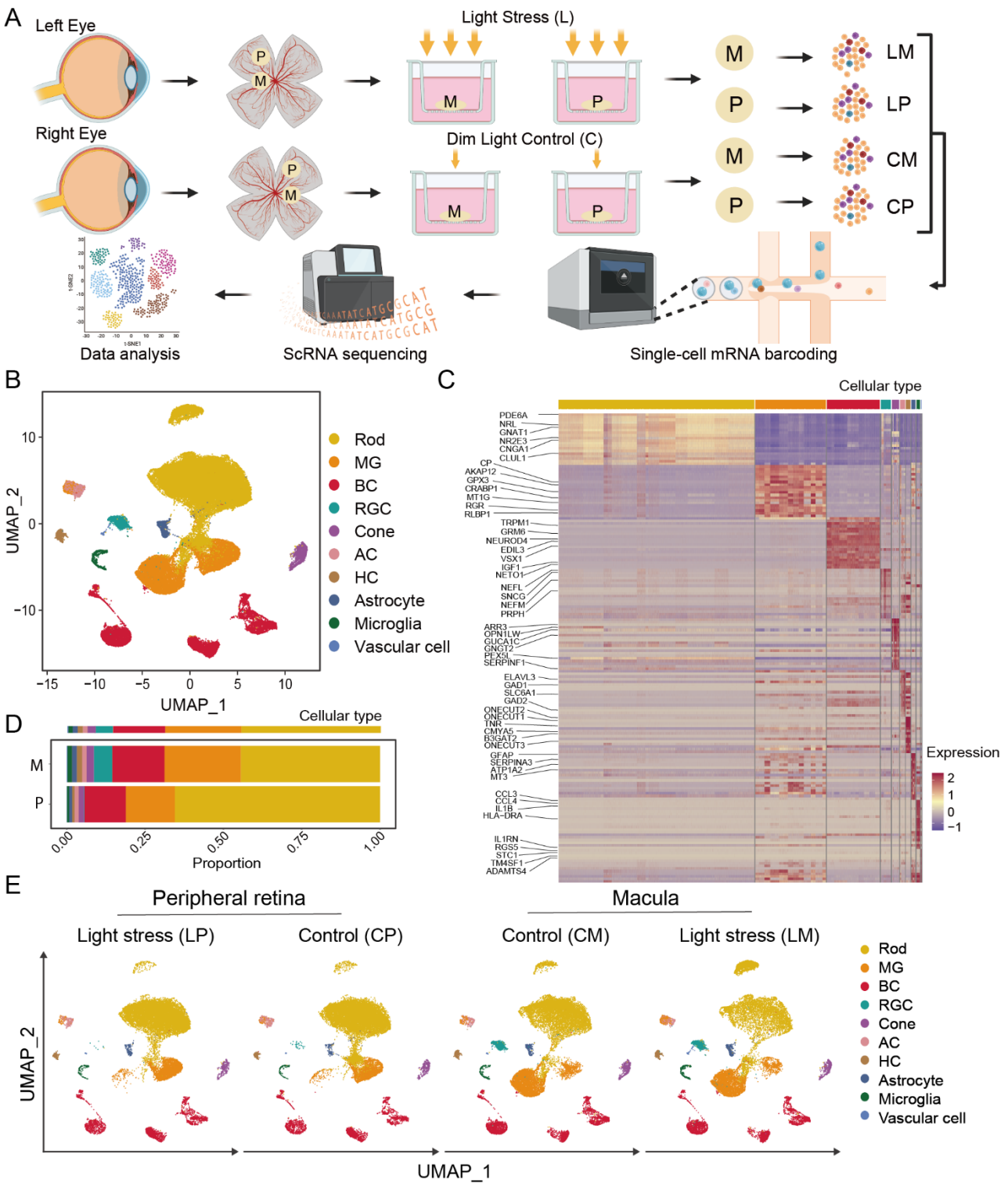

Figure 1. **Schematic workflow for generating single-cell retinal cells and transcriptomic profiles of retinal cells dissociated from the macula and mid-peripheral retina by single cell RNA sequencing analysis**. **A**. The workflow shows the steps involved in generating single cells from human macular and peripheral retinal explants, including exposure to either bright or dim light for 4 hr. The process begins with the dissection of human donor eyes to isolate the neural retina, followed by culturing the macula and mid-peripheral retinal explants on transwells. The retinal cells are dissociated from the tissue to create a single-cell suspension. n=4 donors per treatment group. M: macula, P: peripheral retina, L: light stress, C: dim light, LM: macula with light stress; LP: peripheral retina with light stress; CM: macula with dim light; CP: peripheral retina with dim light. **B**. Retinal cell clustering using UMAP for all transcriptomes detected. **C**. The heatmap of the expression of retinal cell markers in identified cell clusters. **D**. Proportions of retinal cell types in the macula and

peripheral neural retinas. **E**. UMAP for the macula (M) and peripheral retinas (P) with (L) or without (C) light stress.

Transcriptomic changes between the macular and peripheral retinal cells in response to stress

To examine the differential responses of macular and peripheral retinal cells to light stress, we assessed the gene expression changes across all retinal cells in the 4 treatment groups (LP, CP, LM and CM). The Venn diagram (**Figure 2A)** illustrates the number of genes significantly altered after light stress in the peripheral retinas (blue circle: 332 genes) and the macula (orange circle: 159 genes). 47 genes were differentially expressed in both the peripheral retina and macula in response to light stress, while 876 genes were differentially expressed between the peripheral retina and macula without light stress. The correlation analysis found that the peripheral (LP vs. CP) displayed significantly more transcriptomic changes than macula (LM vs. CM) in response to light stress (**Figure 2B**). In this heatmap, a higher correlation (red colour) represents fewer changes.

We divided the overall changes shown in the heatmap into different clusters of retinal cell types to explore cell-type-specific responses to stress in the peripheral retina (**Figure 2C**) and macula (**Figure 2D)**. We introduced an "alteration score" that measures the quantity and expression level change of signature genes during biological processes to quantify the degree of differential presentation of these cell types after a biological perturbation [11]. Higher alteration scores indicate more significant changes. Peripheral Müller cells and rods had significantly higher alteration scores than macular Müller cells and rods, suggesting that the peripheral retina is more responsive to light-induced stress than the macula. We also observed that amacrine cells in the macula were highly sensitive to light stress, with significant and greater transcriptomic changes than amacrine cells in the peripheral retinas. We also observed hyperglycemic stress induced more transcriptomic changes in the peripheral retina than in the macula and higher alteration scores in the peripheral than in macular Müller cells and rods (**Supplementary Figure 4**). These findings suggest a generalised divergence in stress responses between the macula and peripheral retina.

To further explore the impact of light stress on each cell type, we calculated a light stress-associated relative likelihood (y-axis) for each cell (dots) using a manifold approximated from all cells across the dim light control and light stress groups (**Figure 2E**). Examination of the distribution of these values across the 10 previously identified cell types revealed that Müller cells had a wider range of light stress-associated relative likelihood values than other cell types (**Figure 2E**). We also found that light stress induced more peripheral Müller cells with higher light stress-associated likelihood than macular Müller cells. **Figure 2F** displays the proportion of cell numbers from each cell type that had a high light stress-associated relative likelihood value (> 0.6): rods and Müller cells had the greatest relative likelihood in response to light stress.

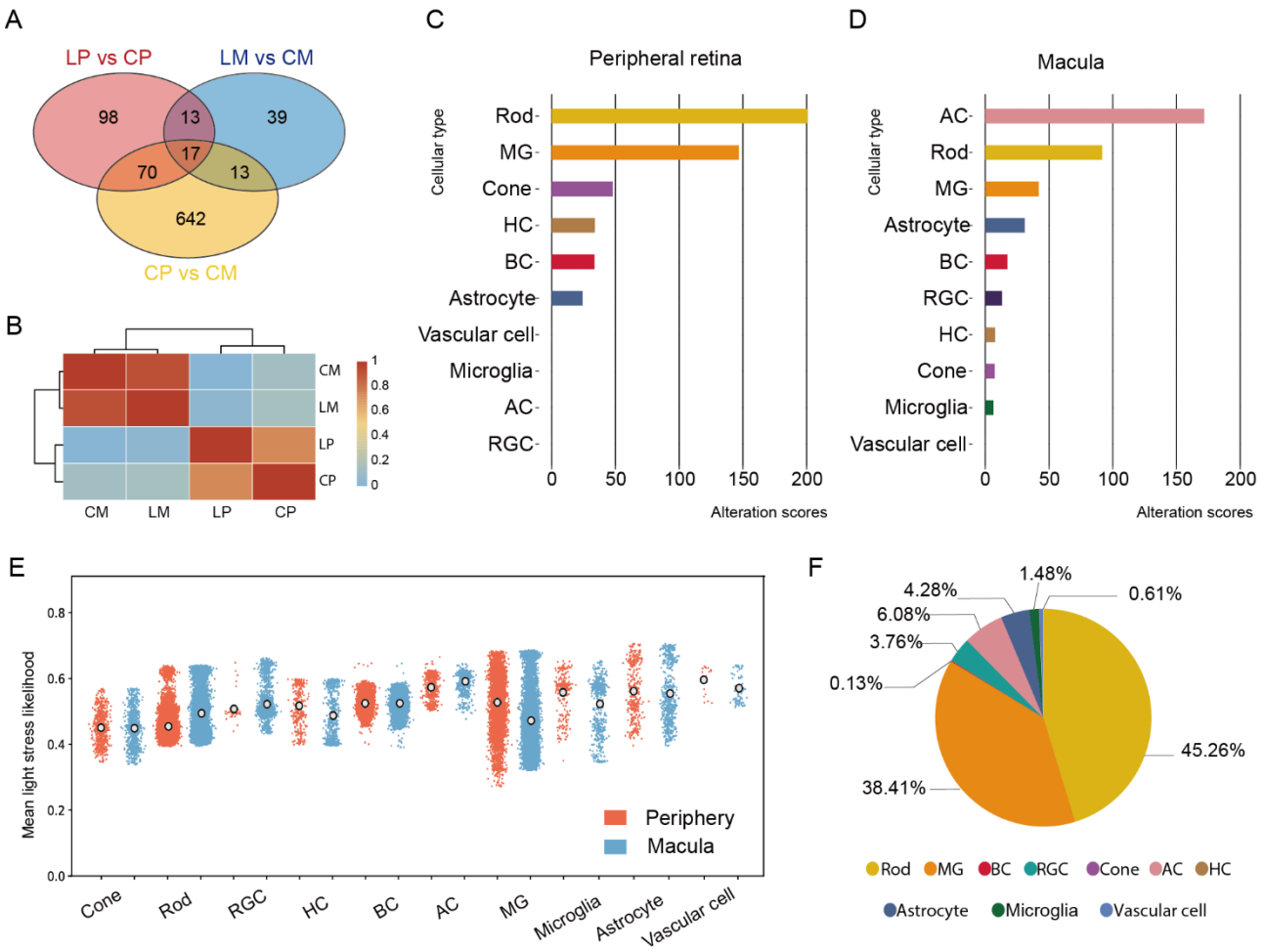

Figure 2. **Regional and cell-type specific alterations in response to stress**. **A**. A Venn diagram illustrates the relationships between LP-CP, LM-CM and CP-CM. **B & C**. Alteration scores of retinal cell types in the macula (**B**) and peripheral retinas (**C**) upon light stress. The higher alteration score indicates more significant changes. In the peripheral retinas, rods and Müller glial (MG) cells have more significant changes; while in the macula, amacrine and rod cells contribute more changes. **D**. A heatmap illustrates the correlations between different treatment groups. High correlation (red) in CM vs LM represents fewer transcriptional changes; low correlation (yellow) in CP vs LP represents significant transcriptomic profile changes. LP: Light stressed Peripheral Müller cells, CP: Control stressed Peripheral Müller cells, LM: Light stressed Macular Müller cells, CM: Control stressed Macular Müller cells. **E**. The scatter plot of all single-cells in the macula and peripheral retinas showing the cell-type distribution of the light stress-associated likelihood values. The grey circles indicated the average likelihoods. **F**. Proportions of each cell type within all cells that has a light stress- associated relative likelihood value greater than 0.6.

Divergent light-induced responses and biological functions of human macular and peripheral Müller cells

We investigated the DEGs between total Müller cells from the macula and peripheral retina after exposure to light stress across the 4 treatment groups (CP, LP, CM and LM) (**Supplementary Figure 5)**. The volcano plot (**Figure 3A**) depicts the top 40 differentially expressed genes (DEGs) that were significantly more highly expressed in macular Müller cells than peripheral Müller cells (displayed on the right) and *vice-versa* (displayed on the left). We subsequently analysed the modulation of these 80 genes under light-induced stress. Red dots in the volcano plot signify genes that experienced a significant 1.19-fold increase under light stress, while blue dots indicate those with a significant 0.91-fold decrease. Our analysis revealed that 25 of the top 40 highly expressed genes in peripheral Müller

cells (left) were significantly differentially expressed in response to light stress (19 genes upregulated and 6 downregulated) in contrast to only 6 of the top 40 highly expressed genes in macular Müller cells (right) (6 downregulated).

We compared the gene expression profiles of macular and peripheral Müller cells to elucidate their functional differences. We selected genes that were expressed more than 1.5-fold higher in the macular (m-HXs) or peripheral Müller cells (p-HXs) (**Supplementary data 2**) and performed a Gene Ontology (GO) analysis with a focus on the response to light stress. Intriguingly, genes that were highly expressed in m-HXs, which showed no transcriptomic changes in response to light stress, were significantly enriched in biological processes related to development of anatomical structure, cell communication, signalling, differentiation and signal transduction (**Figure 3B, Supplementary Figure 5F**) in contrast to p-HXs genes in response to light stress that were substantially enriched in the pathways related to stress responses, including reactions to compounds, metal ions, stress, cell death, metabolic processes, detoxification and regulation of cell death (**Figure 3C, Supplementary Figure 5F**).

Different light-induced responses and biological functions of different subgroups of Müller cells

We identified 6 subtypes (MG1 to MG6) of Müller cells in the transcriptomes obtained from the LP, CP, LM and CM groups (**Figure 3D**). The proportion of 2 major subtypes, macula-dominant Müller glia (MG1) and peripheral retina-dominant Müller glia (MG2), accounted for approximately 75% of Müller cells in the macula and peripheral retinas, respectively (**Figure 3E**). We then focused on 3 subtypes (MG1 to MG3) due to their high abundance, while the MG4 subtype contained relatively fewer cells and MG5 and MG6 were donor-specific (**Figure 3E and Supplementary Figure 5F**). The proportion of MG2 cells in the macula increased more under light stress (LM). This observation suggests that MG2 may play an important role in response to light stress in the retina.

We generated a heatmap to cluster the markers highly expressed in various Müller cell subtypes (**Figure 3F**). MG1 cells had a high expression of feature genes, such as COL4A3, FGF9, DIO2 and ZNF385D, in macular Müller cells [12]. We also found that MG2 expressed genes involved in response to oxidative stress (SOD2, NFKBIA, NFKBIZ, TNFAIP3, BIRC3 and CD44), suggesting that MG2 cells may be strongly associated with retinal pathology. Additionally, MG3 cells expressed several rod markers, namely *RHO*, *PDE6G* and *GNGT1*, along with traditional Müller cell markers. The proportion of MG3 cells expanded slightly within the peripheral retinal samples after exposure to light stress. This finding is consistent with the previous reports that Müller cells have stem cell characteristics that may help regenerate injured or stressed retina [5, 13].

We found that, of all Müller cell subtypes, a significant proportion of MG1 cells had a low likelihood of light stress-associated relative values (**Figure 3G**), indicating that this subset functioned more closely to steady-state Müller cells. MG2 cells had higher values of light stress-associated relative likelihood, suggesting that this population is more responsive to light stress. (**Figure 3H,** red-highly changed).

We performed velocity and trajectory analysis to investigate the transitional relationship between Müller cells and rods. Individual cell velocities were projected onto the UMAP embedding, which was superimposed with Seurat-defined Müller glia subtypes and rods (**Figure 3H**). The Python package PAGA was employed to determine velocity-inferred directionality [14]. We observed a differential trajectory between Müller glia and rods. MG3 exhibited the highest root-like potential and a fast pace of differentiation (**Figure 3I**). This pace was maintained during the production of MG2 cells with high light stress-associated relative likelihood values, which substantially slowed down as the cells became more rod-like (**Figure 3I &J, Supplementary Figure 5G**). These findings indicate a transition trajectory that starts with control-like MG3 cells, followed by light-affected MG3 cells that ultimately result in 3 different endpoints (MG1, MG2 cells and rods). Remarkably, the light

stress associated likelihood increases in correlation with the differential trajectory observed within these three endpoints. However, MG2 cells displayed the most rapid transition pace.

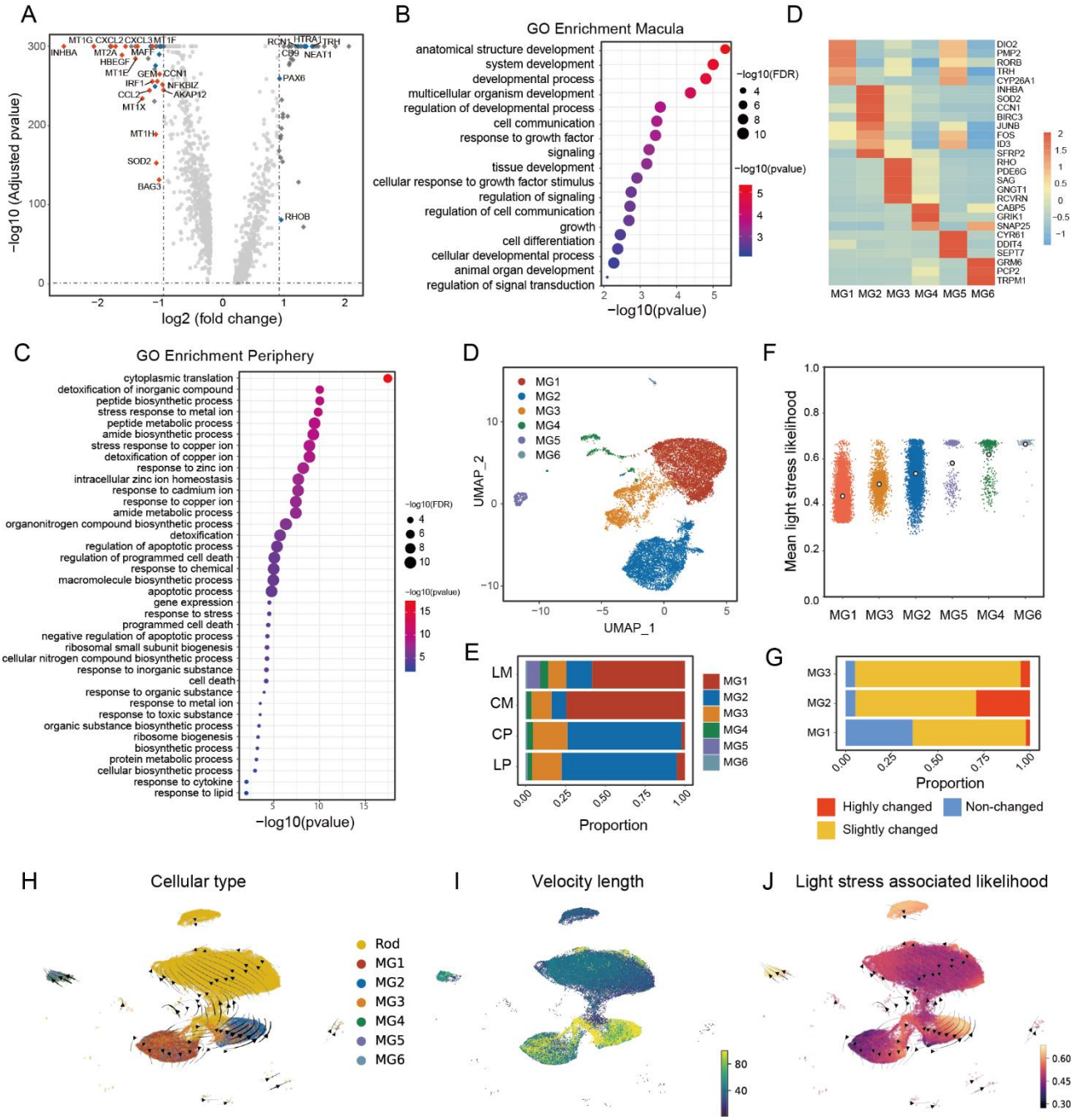

Figure 3. Subclusters of human Müller cells from the macula and periphery retinas. A. The volcano plot of DEGs in Müller cells in the macula and peripheral retinas in response to light stress. **B**. GO analysis of genes highly expressed in macular Müller cells (m-HXs) revealed significant enrichment in biological processes related to cell function and development. **C**. GO analysis of genes highly expressed in peripheral Müller cells (p-HXs) identified significant enrichment in various biological processes related to stress responses. **D**. The UMAP of subclusters of human Müller cells identified from the macula and peripheral retinas. **E**. Proportions of Müller cell subclusters in the macula (M) and periphery (P) with (L) and without (C) light stress. **F**. A heatmap of the cluster with the marker genes highly expressed in various subtypes of Müller cells. **G**. The scatter plot of 6 subtypes of Müller cells revealing the likelihood values of transcriptomes upon light stress. Each dot represents one Müller cell. **H**. Proportions of highly changed (red), slightly changed (yellow) and non-changed (blue) cells in subtypes of Müller cells. **I**. UMAP plot of velocity and trajectory analyse revealed transition dynamics from Müller cells to rods. Colours indicate different cell types. **J**. UMAP

plot of velocity length displaying the speed of differentiation. **K**. UMAP plot of single-cell velocity visualized by the previously calculated light stress associated likelihood values.

Target genes involved in the response to light stress in the periphery-dominant Müller cells.

Given the significantly different responses to light stress that we observed between MG1 and MG2 cells, we investigated the top target genes that were region-specific and associated with pathological processes. We selected the top 10 genes that exhibited differential expression between MG1 and MG2 with or without light stress (**Figure 4A**). Substantial transcriptomic changes were observed in MG2 cells in response to light stress in contrast to MG1 cells which had minimal changes. Among the top 10 genes highly enriched in MG2, *MT1F*, *AKAP12*, *MT1X*, *CCN1*, *MT1E*, *MAFF*, *MT1G* were upregulated in response to light stress. These findings indicate that Müller cells in the human retina consist of distinct subtypes with unique transcriptome profiles exhibiting differential stress responses. We chose the 3 top DEGs, *MT1*, *AKAP12* and *MAFF*, which were particularly abundant in MG2 (**Figure 4B**) and were highly responsive to light stress (**Figure 4C,** highly changed), for further study.

Protein expression patterns of the 3 top DEGs, *MT1*, *AKAP12* and *MAFF*, in the human retina, were studied with immunofluorescent staining. We found that MT1 primarily co-localised with CRALBP, a Müller cell-specific marker, with its expression spanning the entire cell body throughout the neural retina (**Figure 4D-F**). MT1 was also expressed in the cell bodies of neurons in the inner nuclear layer. AKAP12 staining co-localised with CRALBP in the retinal nerve fibre layer, outer plexiform layer and outer limiting membrane of the peripheral retina (**Figure 4G-I**). We observed MAFF staining in ganglion cells, Müller cells and photoreceptors (**Figure 4J-L**). We validated the protein expression of *AKAP12*, *MT1* and *MAFF* using freshly obtained retinal tissue punches collected from different locations across the human retina (**Supplementary Figure 1**). The protein expression of these genes was consistent with the distinct expression patterns identified in our RNAseq analysis, with lower expression levels observed in the macula than that in the peripheral retina.

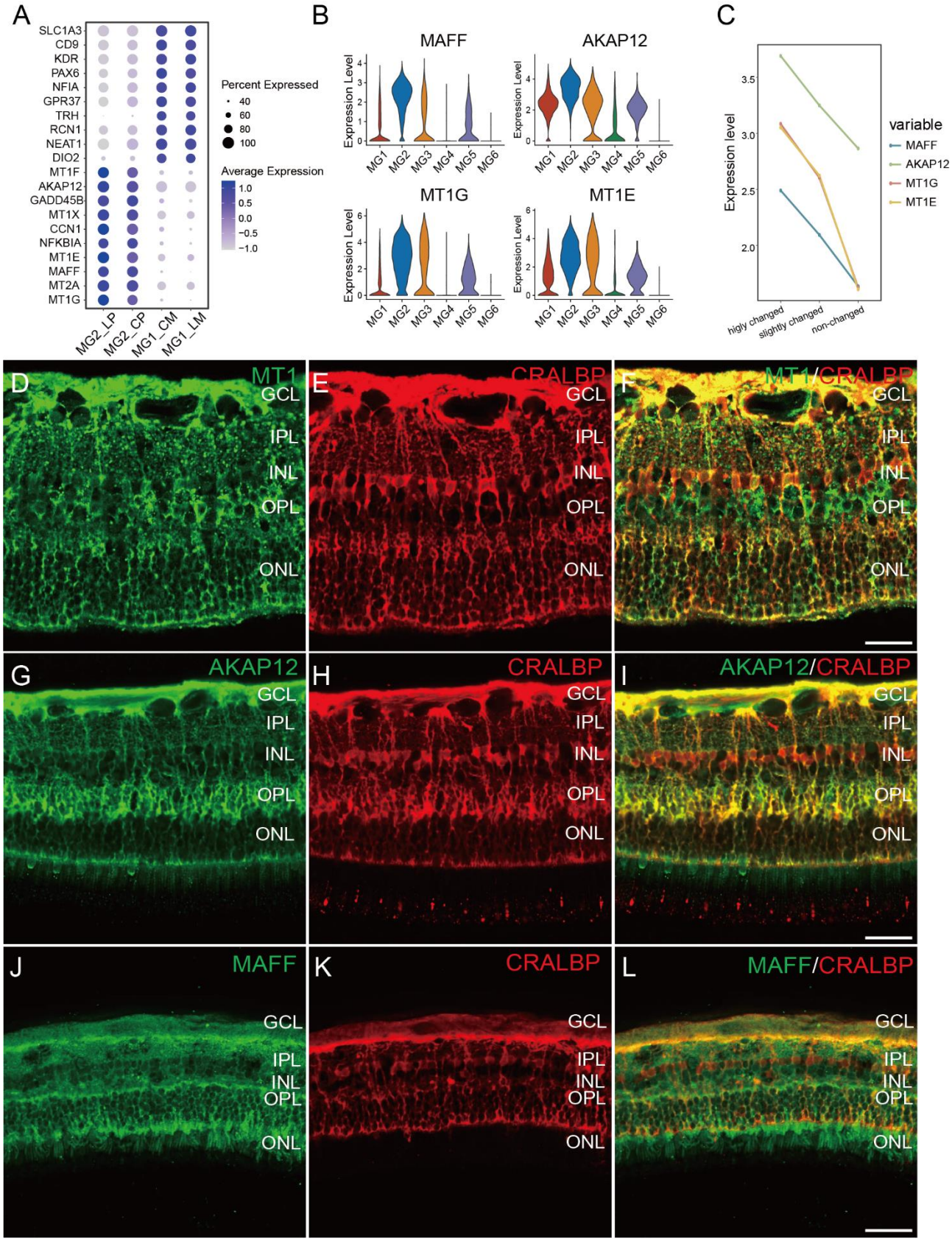

Figure 4. Immunofluorescent (IF) staining of MT1, AKAP12 and MAFF in human retina.

A. Dot plot illustrating the top 10 DEGs between MG1 cells and MG2 cells in response to light stress. **B**. The violin plot showing the expression level of *MT1*, *AKAP12* and *MAFF* in subtypes of Müller cells. **C**. The line chart showing the average expression level of *MT1G*, *MT1E*, *AKAP12* and *MAFF* in MG2 cells in response to light stress. **D**. The IF staining of MT1 (green) in the peripheral retina.

E. The IF staining of CRALBP (red), a Müller cell marker. **F**. Co-localization of MT1 and CRALBP in human retina. **G**. The IF staining of AKAP12 (green) in the human peripheral retina. **H**. The IF staining of CRALBP (red). **I**. Co-localization of AKAP12 and CRALBP in human retina. **J**. The IF staining of MAFF (green) in the peripheral retina. **K**. The IF staining of CRALBP (red). **L**. Co-localization of MT1 and CRALBP in human retina (arrows). Scale bar=50µM

Functional Validation of *MT1*, *AKAP12* and *MAFF* in Müller Cells In Response to Light Stress

We knocked down *MT1*, *AKAP12* and *MAFF* in primary human Müller cells under light stress with siRNA (**Figure 5A**). Knockdown of *AKAP12* or *MAFF* but not *MT1* reduced cell viability by 5-10% compared with control cells under dim light (**Figure 5B**). Under light stress, by contrast, the viability of Müller in which *MT1*, *AKAP12* or *MAFF* had been knocked down decreased by 10-30% compared with control (**Figure 5C**).

We also evaluated the mitochondrial membrane potential of primary Müller cells using JC-1 staining. The JC-1 ratio (J-aggregate/Monomer) was not significantly different between the control and *MT1*, *AKAP12* and *MAFF* knockdown groups under dim light (**Figure 5D**). However, the JC1 ratio of the *MAFF* knockdown group was significantly lower than that of the control group under light stress (**Figure 5E**). These findings suggest that *MAFF* may play an important role in the Müller cell stress response.

To gain further insights into the function of these genes, we performed bulk RNA sequencing in Müller cells with *MT1*, *AKAP12* and *MAFF* siRNA silencing, with or without light stress. The mRNA levels of *AKAP12*, *MAFF* and *MT1G* were significantly reduced, as shown in the volcano plots (**Figure 5F-H,** blue circles). Heatmaps of gene expression between *AKAP12*, *MAFF* and *MT1G* siRNA silenced groups and the control group displayed distinct clustering of individual samples within the same group (**Supplementary Figure 6**).

IPA analysis revealed several significant differences in canonical pathways that were impacted by *MT1*, *AKAP12*, or *MAFF* knockdown. The commonly altered pathways included mitochondrial dysfunction, protein kinase A signalling and NAD signalling (**Figure 5I-K**). Pathways associated with mitochondrial dysfunction were activated in all three target gene knockdown groups, while pathways related to protein kinase A and NAD signalling pathways were inhibited.

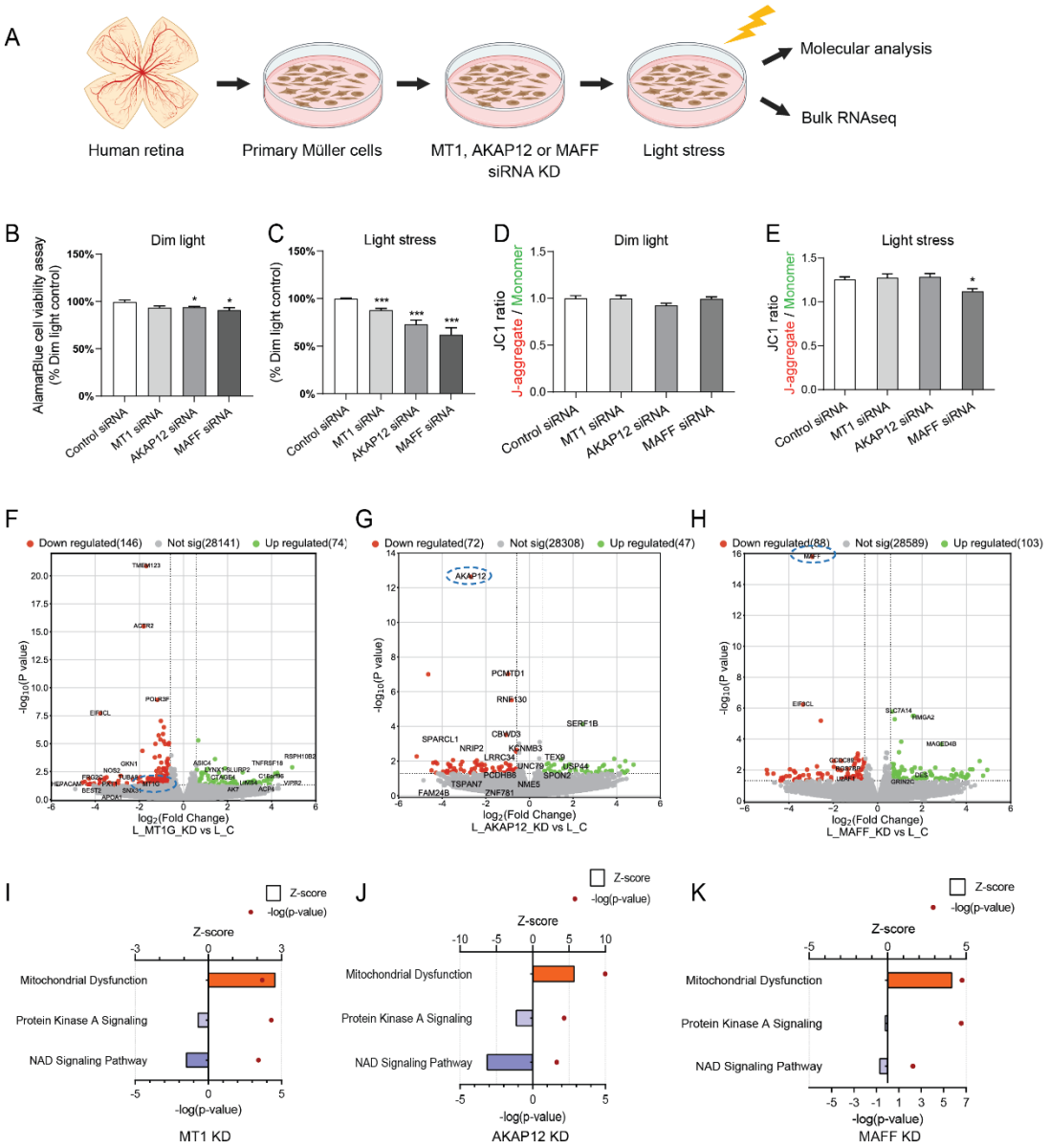

Figure 5. Knockdown of *MT1*, *AKAP12* and *MAFF* in human primary Müller cells. A. *MT1*, *AKAP12* and *MAFF* siRNA knockdown in the primary Müller cells exposed to light stress. **B** & **C**. AlamarBlue cell viability assay on primary Müller cells with or without *MT1*, *AKAP12* and *MAFF* siRNA silencing in response to light stress. n=6 per group. *p<0.05, *** p<0.001, significantly different as indicated, one-way ANOVA followed by Dunnett's multiple comparisons test. The data are presented as means ± standard error of mean (SEM). **D** & **E**. JC1 assay on primary Müller cells with or without *MT1*, *AKAP12* and *MAFF* siRNA knockdown in response to light stress. n=8 per group. One-way ANOVA followed by Dunnett's multiple comparisons test. **F-H**. The volcano plots of differential gene expression ($p < 0.05$, FC > 1.5) in *MT1G*, *AKAP12* and *MAFF* siRNA knockdown vs control groups. **I-K**. IPA of differential gene expression in human primary Müller cells with *MT1G*, *AKAP12* and *MAFF* siRNA knockdown than that of the control group in response to light stress.

Activation of *AKAP12* and *MT1* in Human Diabetic Retinopathy and in a Mouse Model of Subretinal Neovascularization

We analysed the expression of *AKAP12* and *MT1* in a *postmortem* human retina with documented diabetic retinopathy (DR) (**Supplementary Figure 7**). We found patchy upregulation of *AKAP12* in the retinal nerve fibre layer, inner plexiform and nuclear layers, the processes of Müller cells in the

outer plexiform layer and in the walls of intraretinal cysts (**Figure 6A**). Higher magnification images demonstrated significant *AKAP12* activation in Müller cell processes surrounding photoreceptors in the outer nuclear layer (**Figure 6B**). The expression of *MT1* was also elevated in the walls of intraretinal cysts (**Figure 6C)**. A higher magnification view illustrated the specific region in the retina with macular edema where *MT1* activation was found (**Figure 6D**). These findings implicate AKAP12 and MT1 in the pathophysiology of DR.

Next, we examined the protein expression of *AKAP12*, *MT1* and *MAFF* in JR5558 mice spontaneously developing bilateral subretinal neovascularisation [15]. Subretinal lesions appeared around 4 weeks and became established at 8 weeks, as confirmed by colour fundus photography, optical coherence tomography and fundus fluorescein angiography (**Figure 6E-G**). We compared the protein expression of *AKAP12*, *MT1* and *MAFF* in the JR5558 mouse retina with the C57BL/6 control retina. We found that AKAP12 was upregulated at both 4 weeks and 8 weeks of age in the JR5558 mouse retina compared with the control retina (129% vs 100%, 169% vs 100%) (**Figure 6 H&I**). The protein expression of *MAFF* and *MT1* was significantly greater at 8 weeks of age in the JR5558 mouse retina than in the control (217% vs 100%, 121% vs 100%, respectively). These results show that the stress-responsive genes *AKAP12*, *MAFF* and *MT1* are activated in subretinal neovascularisation, which is a common vision-threatening mechanism in retinal disease.

Overall, our findings demonstrate that *AKAP12* and *MT1* are activated in human diabetic retinopathy. *AKAP12*, *MAFF* and *MT1* were activated in a mouse model of subretinal neovascularisation, highlighting their potential roles in the pathophysiology of these retinal diseases.

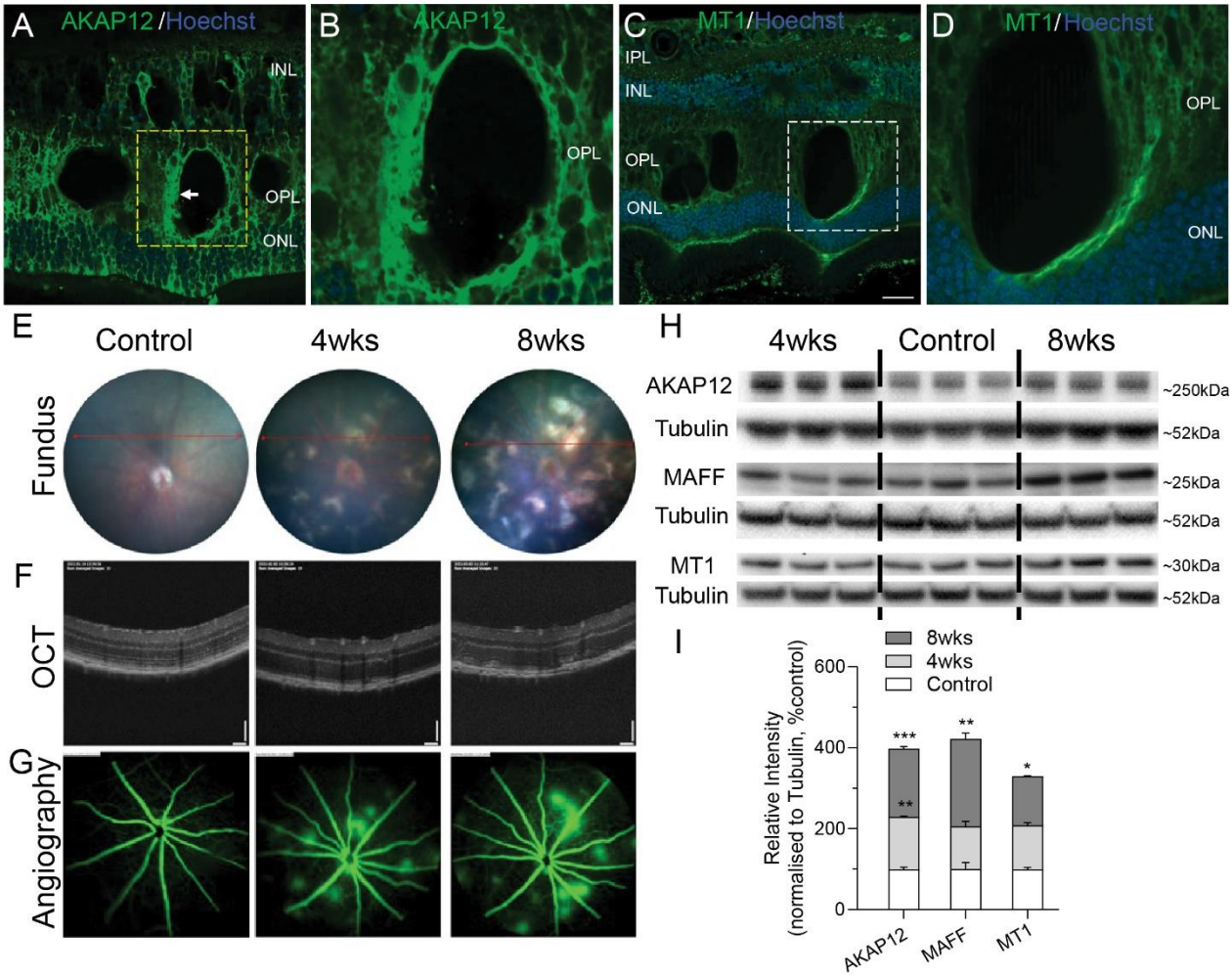

Figure 6. Activation of *AKAP12* and *MT1* in human retina with DR and *AKAP12*, *MT1* and *MAFF* in JR55558 mice mimicking wet AMD. A. The IF staining of AKAP12 (green) and Hoechst (blue) on the doner retina with DR. **B**. Magnified image in the yellow dotted box of **A**. **C**. The IF

staining of MT1 (green) and Hoechst (blue) on the donor retina with DR. **D**. Magnified image in the white dotted boxes of **C.** Scale bar=50µM**.** The fundus photo (**E**), OCT (**F**) and FFA (**G**) images of the C57BL/6J control and JR5558 mice at 4 and 8 weeks old of age. **H & I**. Images of representative protein bands and the corresponding densitometry analysis of Western Blot against AKAP12, MAFF and MT1 in the retinas of both control and JR5558 mice at the ages of 4 and 8 weeks. n=3 mouse retinas per group. *p<0.05, **p<0.01, ***p<0.001. One-way ANOVA followed by Dunnett's multiple comparisons test.

Discussion

Though Müller cells are found in both the macula and the peripheral retina, disparities exist in their distribution, density, morphology and molecular functions across these regions [6]. This study examined the stress responses of Müller cells in both areas utilising scRNAseq on human macular and peripheral retinal explants. Macular Müller cells had minimal transcriptional changes in response to stress compared to their peripheral counterparts. Analysis of the top three genes most abundantly expressed in peripheral Müller cells revealed a crucial role in cellular survival under stress. Our findings indicate a previously unobserved distinction between macular and peripheral Müller cells, which might offer insights into the selective vulnerability of the macula in specific retinal diseases such as AMD and MacTel.

Metallothionein (*MT*) refers to a group of low molecular weight, cysteine-rich proteins that play critical roles in various biological processes, including metal metabolism [16], protection against DNA damage [17] and regulation of apoptosis [18, 19]. *MT1* has been implicated in age-related neurodegeneration [20, 21], as it is associated with aging and endoplasmic reticulum (ER) stress, particularly in defending against nitric oxide (NO)-induced stress. NO-induced stress in Müller cells has been implicated in the development of various retinal conditions, such as DR, glaucoma and AMD [22].

AKAP12 interacts with a variety of key kinases, such as PKA and PKC, which are essential for the proper regulation of morphogenetic cell movement [23]. *AKAP12* is involved in maintaining vascular integrity and regulating endothelial cell function [24-26]. It has been identified as a maturation factor for the blood-brain barrier (BBB) that alleviates damage and dysfunction of the BBB caused by ischemic stress [27]. Although the specific function of *AKAP12* in human Müller cells remains largely unclear, the elevated expression in Müller cell processes that we observed surrounding areas with apparent intraretinal fluid in the retina observed in DR suggests its potential association with the response of Müller cells to retinal pathology.

MAFF protein belongs to the small Maf family of proteins that are known to form heterodimers with Nrf2, thereby modulating the transcriptional activity of downstream genes [28]. There is limited information regarding the specific role of *MAFF* proteins in human diseases, but they have been implicated in various pathological conditions such as cancer, diabetes, immune system disorders and neurodegenerative diseases such as Alzheimer's disease and Parkinson's disease [29-33]. The role of *MAFF* in Müller cells has not been previously investigated. However, its high expression in Müller cells suggest it may modulate the Nrf2-related stress response in these cells. Future study is warranted to elucidate the roles of MAFF in Müller cells and other biological processes, this is beyond the scope of the current study.

MT1, *AKAP12* and *MAFF* are much more strongly expressed in Müller cells of the peripheral retina than of the macula. siRNA knockdown of these genes in human primary Müller cells disrupted multiple stress response signalling pathways, including mitochondrial function and the protein kinase A and NAD signalling pathways. A better understanding of how the macula responds to stress when it only expresses stress response genes weakly and non-inducibley may pinpoint new treatment targets for macular diseases.

Macular Müller cells have a distinct phenotype, with a lower expression of stress response genes than Müller cells from the peripheral retina. This unique phenotype may offer an evolutionary

advantage by preserving the normal function of the macula under stress, thereby maintaining central vision during sudden environmental changes and increasing survival chances in harsh conditions. Cellular stress responses typically promote cell survival, but may also compromise normal cellular functions [34]. An acute stress response in Müller cells might disrupt their ability to effectively regulate neurotransmitter levels, leading to an imbalance in the retinal chemical environment and short-term vision impairment. Through minimising their stress response, macular Müller cells may have evolved to suppress their stress response in favour of maintaining their normal function under acute stress to preserve central vision in a rapidly changing environment. This adaptation would have been beneficial in evolution when central vision was critical for as hunting, foraging and evading predators. The capacity to maintain clear central vision during abrupt changes in lighting condition would have substantially enhanced their chances of survival in harsh conditions.

Studying the macula is challenging because laboratory animals do not have maculas apart from non-human primates which raise ethical issues. We addressed this by using *postmortem* human retinal/macular explants to investigate the stress response of the human macula. The data derived from this model system complements other models utilised in retina research, such as mice and organoids. One of the primary advantages of using human retinal explants is the direct examination of gene expression and morphology of the human macula in its entirety. Inherent limitations of this system include the lack of a functional vascular network and interaction with the retinal pigment epithelium (RPE). These disadvantages could potentially be addressed with perfusion and co-culture systems. The use of postmortem tissue may raise concerns regarding viability and metabolic activity, but there is growing evidence to support the functionality of cultured human retinal explants despite *postmortem* delay.[11]. We have previously reported that the metabolic features of human retinal explants at least as good as those of mouse retinas and retinal organoids [35].

Our use of acute intense light exposure as a model for the chronic stress associated with aging may not perfectly reflect the true *in vivo* response of the human macula and peripheral retina. Despite this, our method is a valuable starting point for investigating the stress response of the macula. It sets the stage for future, in-depth research on neurotoxins, such as deoxy-sphinganine (unpublished data), that significantly influence the pathogenesis of macular telangiectasia type 2 [36], and it helps us begin to unravel the distinct ways the macula responds to stress.

In conclusion, we observed that macular Müller cells exhibit a subdued response to stress, possibly due to the higher functional demands placed on them in the macula region. These cells express low levels of several key stress-response genes that significantly contribute to the resilience of peripheral Müller cells under stress. Future investigations are needed to clarify further the molecular mechanisms underlying the distinct stress response characteristics of macular Müller cells. Our findings indicate that this reduced stress response in macular Müller cells could offer an evolutionary advantage by allowing these cells to sustain their normal functions even under acute stress.

Materials and Methods

Tissue Collection and Retinal Dissection

The use of donated human eyes was approved by the Human Research Ethics Committee of the University of Sydney (Protocol Number: 2016/282 and X21-0208 & 2020/ETH03339). Donors had no known eye diseases. Retinal dissection was conducted as previously described [37]. In brief, donor eyes were acquired from the New South Wales Tissue Bank after the corneas had been removed for transplantation. The donor issues were preserved in CO_2-independent medium at 4 °C until they were dissected. For dissection, the eye was placed on a petri dish and the iris, lens and vitreous were excised from the eyecup. The neural retina was then carefully detached from the underlying retinal pigment epithelium and transferred to a fresh petri dish. Circular retinal tissues with a diameter of 5mm were collected from the macula or mid-peripheral region of the superior retina by punch biopsy (#BP-50F, Kai Medical) and processed for downstream assays. The mid-peripheral region was identified as the midpoint between the fovea and ora serrata. 2mm-diameter circular retinal samples extending from the fovea to the superior and inferior peripheral neural retina (**Supplementary Fig1A**) were collected and extracted for protein analysis. One postmortem eye from a donor with diabetic retinopathy (DR) was used to validate the expression of target genes in the diseased retina. Detailed fundus photography was conducted to document characteristics and features present within the diseased retina.

Light and High Glucose Stress Models on Retinal Explants and Human Primary Müller Cells

We employed a custom-built light exposure system situated within the tissue culture incubator to induce light stress in retinal explants and human primary Müller cells (**Supplementary Fig2**). Light stress was accomplished by subjecting explants to intense light at 32k lux, while the control group were exposed to 5 lux light. Retinal explant tissues were placed on 12-well plate transwell inserts (#3460, Corning) with neurobasal medium (#21103049, Gibco), 1% B27 (#17504044, Gibco), 1% N2 (#17502048, Gibco), 1% fetal bovine serum (FBS, #F9423, Sigma-Aldrich), 1% GlutaMax (#35050, Gibco), 1%ITS (#51500056, Gibco) and 1% penicillin-streptomycin (P/S, #P4333, Sigma-Aldrich). Macular and peripheral neural retinal explants were exposed to light for 4 hr (Fig1A). Three days after siRNA transfection, human primary Müller cells in 12-well (#3513, Corning) or 96-well plates (#3340, Corning) were exposed to intense (32k lux) or dim (5 lux) light. Macular and peripheral retinal explants were cultured in either normal glucose (5mM glucose, left eye) or high glucose (25mM, right eye of the same donor) on 12-well transwell inserts with DMEM (#10569, Gibco) supplemented with 1% B27, 1% N2, 1% FBS and 1% P/S for 24 hours.

Single Cell dissociation and cDNA library construction

Macular and peripheral explants were dissociated into single cells following light or high glucose treatment as depicted in **Fig1A**. Single-cell dissociation was achieved using the Papain Dissociation System (Worthington Biochem, NJ, USA) according to the manufacturer's protocol. Briefly, the entire retinal explant was immersed in papain solution for 30 minutes at 37 °C, followed by dissociation through pipetting with a glass pipette. The single-cell suspension was combined with barcoded gel beads in a microfluidic chip and run on the Chromium Controller (10X Genomics) to create gel bead-in-emulsion (GEMs) droplets (Chromium Next GEM Single Cell 3′ Kit v3.1, 16 rxns PN-1000268, 10×Genomics). The GEMs were incubated, enabling mRNA reverse transcription into cDNA. The barcodes from the gel beads were incorporated into the cDNA molecules by uniquely tagging the cDNA originating from each individual cell. The barcoded cDNA was then amplified using PCR to construct a library. The libraries were sequenced on an Illumina NovaSeq 6000 platform.

Single Cell RNA sequencing data analysis

The raw sequencing data was processed by the Cell Ranger software (v3.0.2, 10x Genomics). A human reference genome (GRCh38) was used to accurately map the sequencing readouts and quantify gene expression. We then applied Seurat (v4.1.1) [38] to perform the pre-processing and downstream analysis of the single-cell gene expression data. Cells with an expression of unique feature counts over 6,000 (as for the high glucose treated group, this parameter was 10,000) or less than 200, a mitochondrial gene ratio over 15% and a hemoglobin gene ratio over 5% were filtered out. DoubletFinder [39] (v2.0.3) was used to detect and remove the doublets as to the following criteria: pN = 0.25, pK = 0.09, PCs = 1:20, sct = TRUE and reuse.pANN = FALSE. After the above quality control, we normalised and log-transformed the featured expression measurements for each cell. 2,000 highly variable features were chosen for downstream data scaling. The integration of multiple single-cell datasets from different biological contexts was implemented by SeuratWrappers (v 0.3.0) with LIGER algorithm. It depends on integrative non-negative matrix factorisation to delineate shared and dataset-specific factors of cell identity [40]. Then the "FindNeighbors" and "FindClusters" functions were applied for unsupervised clustering. For visualization, UMAP (Uniform Manifold Approximation and Projection) was used to reduce the dimensionality. We further annotated each cell cluster based on specific marker gene expression. The differentially expressed genes were calculated by the "FindMarkers" function with specific settings (only.pos=FALSE, min.pct=0.2, logfc.threshold = 0.2)

Calculating the Alternation Score of different cell types

To quantify the change in cellular response to light, we designed the Alternation (AC) Score. The first step of selecting the signature genes was conducted as a previously published method that characterized the MI contribution [41]. However, we have modified the second step to calculate both the quantity and expression level change of signature genes during the light stress process. Here, we defined the new AC_{score} as follows:

$$AC_{score(j)}=SUM\ log2(FC_{\exp(i)} \cdot FC_{prop(i)} + 1) \quad (1)$$

In which $FC_{exp(i)}$ refers to the expression fold change of the ith signature gene in the jth cell type between the light stress and control groups, $FC_{prop(i)}$ is the proportion fold change of the cells that express the ith signature gene between the light stress and control groups in the jth cell type.

Light stress-associated relative likelihood analysis

MELD algorithm implemented in Python (v.3.8.16) was employed to calculate the continuous light stress-associated relative likelihood of each cell across the entire single-cell dataset [42]. In brief, the density of each sample (replicates and conditions) was estimated on a MELD graph built over the cellular transcriptomic state space (beta=67, knn=7). We then compared the density estimates between strong and dim light conditions within each replicate. The resulting relative likelihoods across replicates were normalized to quantify the probabilities of a given cell would be observed in the light stress condition. Cut-offs of values greater than 0.6 and less than 0.4 were used to determine whether a cell was enriched, depleted, or unchanged.

Single-cell Trajectory Analysis

We utilized the 10×velocyto pipeline on the filtered cell ranger-generated BAM files to determine the number of spliced and unspliced reads for each sample. Then, we employed the dynamical model of scVelo v.0.2.3 [43] for single-cell RNA velocity inference. We obtained a comprehensive view of RNA velocity across all genes and cells by visualizing a vector field on top of the 2D dimensional reduction plot. We enhanced our interpretation by leveraging partition-based graph abstractions (PAGA) to ascertain the directionality between cells.

Gene Ontology Analysis

Gene Ontology (GO) analysis was conducted using the web-based resource, the Generic Gene Ontology Term Finder [44], accessible at https://go.princeton.edu/cgi-bin/GOTermFinder. Highly expressed genes in macula-dominant Müller glia (m-dMG) were defined as "m-HXs". Highly expressed genes in peripheral retina-dominant Müller glia (p-dMG) were defined as "p-HXs". Light-induced Changes were defined as "LiC". GO analyses were performed on the m-HXs and p-HXs (fold change >1.5,) with (adjusted p value <0.05) or without LiC (adjusted p value >0.05).

Ingenuity Pathways Analysis

QIAGEN Ingenuity Pathways Analysis (IPA) was performed to identify significant canonical pathways and predict which pathways are activated or inhibited between control and MT1, MAFF and AKPAP12 siRNA treatment groups. Upregulated and downregulated genes were imported into the IPA software and subjected to core analysis to identify canonical pathways.

Vibratome sectioning

Human retinal tissue from the macula and mid-periphery was obtained using a 5mm-diameter biopsy punch after separating the neural retina from the RPE-choroid-sclera eyecup. Tissues were fixed in 4% paraformaldehyde for 1 hour and then washed with 1× phosphate-buffered saline (PBS). Retinal tissues were embedded in 3% low-melting agarose (#50100, Lonza) within a plastic cubic mould. The tissue blocks were secured onto the specimen plate of a vibratome (#VT1200S, Leica). Serial tissue sections, 100µm thick, were generated through vibrating sectioning. The tissue slices were maintained in cold 1× PBS until further use.

Immunofluorescent staining and imaging

Retinal slices were blocked overnight in blocking buffer (5% normal donkey serum and 0.5% Triton-X100 in PBS) in a 48-well plate (#3548, Corning). Primary antibodies (**Table 1**) were diluted in 1% normal donkey serum and 0.5% Triton-X100 in PBS. Tissues were incubated in primary antibody for consecutive 5 days, then washed three times with PBS and placed in a diluted secondary antibody (1% normal donkey serum and 1% Triton-X100 in PBS) for two days. Tissues were then washed 3 times with PBS. Nuclei were stained with Hoechst 33342 for 30 minutes in the dark. Slices were mounted onto polysine-coated slides (Menzel Glaser, Germany) with secure-seal spacers (ThermoFisher Scientific, MA, USA) using VECTASHIELD mounting medium (#H-1000, Vector Laboratories). Confocal images were taken using a confocal microscope and imaging system (Zeiss LSM700). Zen Software (blue edition) from Zeiss was used to analyse the images.

Western Blot

Samples of 2mm diameter retinal punches were collected from donor eyes (**Supplementary Figure 1A**) and homogenized on ice using radio-immunoprecipitation assay (RIPA) buffer (#900000064244, Merck) supplied with phosphatase and protease inhibitor (1:100, #5872S, Cell Signaling Technologies). Human primary Müller cells were lysed in RIPA buffer with phosphatase and protease inhibitor in a 12-well plate. Tissue and cell lysate were centrifuged at 12,000 g at 4°C for 15 minutes. Supernatants were collected and aliquoted. Protein concentration was determined using a BCA assay kit (#QPBCA, Sigma-Aldrich). Protein samples were mixed with DTT (#D9779-10G, Sigma) and

loading sample buffer (#NP0007, Invitrogen), heated at 75°C for 10 minutes and then cooled on ice for two minutes. Samples were loaded onto the 3-8% Tris acetate gel (#EA03785BOX, Invitrogen) for AKAP12 evaluation and electrophoresed at 150 V, 4 °C for 60 minutes. Samples were loaded onto 10-20% Tricine gels (EC66255BOX, Invitrogen) for the evaluation of MAFF and MT1 and were electrophoresed at 125 V, 4 °C for 90 minutes. Proteins were transferred onto PVDF membranes (#IEVH85R, Millipore, USA) using the wet transfer system (#1703930, BioRad, USA), following the manufacturer's instructions. PVDF membranes were blocked with 5% bovine serum albumin (BSA, #A9647-100G, Sigma) in 1×tris-buffered saline (TBS) for one hour at room temperature and then incubated with primary antibodies (**Table 1**) diluted in 1% BSA in tris-buffered saline with tween 20 (TBST) overnight at 4°C. Membranes were then washed three times with TBST and incubated with secondary horseradish peroxidase (HRP)-antibodies in 1% BSA in TBST for 2 hr. Membranes were then washed three times with 1×TBST and twice with 1×TBS. Protein bands were visualised using Clarity ECL substrate (#170-5061, BioRad) and photographed using the G-Box imaging system (In Vitro Technologies). The specific bands of interest were quantified using the GeneTools image scanning and analysis package. Protein expressions were normalised to α/β tubulin.

siRNA treatment

Human primary Müller cells were cultured and passaged following the method described previously [9]. Human primary Müller cells (P3) at 80% confluency were transfected with *MT1* (assay ID: s194623, ThermoFisher Scientific), *AKAP12* (assay ID: s18435, ThermoFisher Scientific), *MAFF* (assay ID: s24370, ThermoFisher Scientific) and control small interfering RNA (siRNA) (assay ID: 4390843, ThermoFisher Scientific) at a concentration of 10nM using Lipofectamine 3000 (#L3000-008, Invitrogen), following the manufacturer's instructions. Müller cells were treated with siRNA in either 12-well or 96-well plates for three days, reaching 100% confluency prior to further experiments.

AlamarBlue assay

Human primary Müller cells (P3) were transfected with *AKAP12*, *MT1*, *MAFF* and control siRNA in a 96-well plate for three days, then starved overnight and exposed to light stress for four hours. Cells were treated with AlamarBlue reagent (1:10 dilution, #DAL1100, ThermoFisher Scientific) and incubated at 37 °C for 4 hr using the AlamarBlue cell viability assay kit. The fluorescence was then read using the microplate reader (Fluostar Omega, BMG Labtech) with the 544nm excitation wavelength and 590nm emission wavelength.

JC1 assay

Human primary Müller cells (P3) after siRNA treatments were incubated with JC-1 dye (#T3168, Invitrogen) at a concentration of 1.0 μg/mL in DMEM at 37 °C for 30 minutes to measure the mitochondrial membrane potential. The medium was replaced with Hanks' balanced salt solution (HBSS) and fluorescence was measured using a plate reader. The fluorescence was detected with the 475nm excitation wavelength and 530nm for green emission and 590 nm for red emission. The ratio of red fluorescence divided by green fluorescence of each sample was calculated. All data were normalised to the control siRNA treatment group.

mRNA extraction, bulk RNA sequencing and bioinformatic analysis

Total mRNAs were extracted from human primary Müller cells treated with *AKAP12*, *MT1*, *MAFF* and control siRNA using the GenEluteTM Single Cell RNA Purification Kit (#RNB300, Sigma-Aldrich), following the manufacturer's instructions. The concentration of mRNA was determined using the Qubit RNA HS Assay Kit (#Q32852, Invitrogen). The extracted mRNA samples were sent

to Novogene (Singapore) for bulk RNA sequencing after quality control assessment. The library was prepared and a 150 bp paired-end sequencing strategy was used to sequence the samples. The quality of the library was analysed using the Agilent Bioanalyzer 2100 system.

Mouse eye examinations and retinal tissue collection

Approval for all experimental procedures was obtained from the University of Sydney Animal Ethics Committee, ensuring adherence to ethical standards and the welfare of animals (Project number: 2021/2013). JR5558 mice (strain #:005558; RRID:IMSR_JAX:005558) derived from The Jackson Laboratory were used for the validation of protein expression of AKAP12, MT1 and MAFF. C57BL/6J wild-type mice were used as the control. Color fundus images were captured using the Phoenix-Micron imaging system to showcase the retinal lesions (Phoenix MICRON IV). Their corresponding transverse images were captured to reveal the layers and structures of retinal lesions using optical coherence tomography (Phoenix MICRON OCT2). Fundus fluorescein angiography (FFA) was conducted to evaluate retinal vasculature and perfusion using the Phoenix-Micron imaging system (Phoenix MICRON IV). All scans were conducted at 4 and 8 weeks on both JR5558 and C57BL/6J mice. Mouse retinal tissues from both 4 and 8 weeks were collected for protein extraction at 4 and 8 weeks of age. Western blot was conducted for validations of protein expression of *AKAP12*, *MT1* and *MAFF*.

Statistical analysis

Each in *vitro* experiment was independently conducted at least three times from three donors, with more than six replicates per group. The western plot for mouse samples was performed using three independent samples in each group. The data are presented as means ± standard error of mean (SEM). One-way ANOVA followed by Dunnett's multiple comparisons test was performed using GraphPad Prism version 10.0.2 for Windows, GraphPad Software, Boston, Massachusetts USA. A significance level of $p < 0.05$ was adopted to indicate statistical significance.

Table 1. List of Antibodies Used in the Study

Antibodies	Source	Catalogue NO.	Host	Dilutions	
				WB	IF
α/β-Tubulin	Cell signalling	#2148	Rabbit	1:1000	N/A
CRALBP	Abcam	AB15051	Mouse	N/A	1:500
MAFF	Abcam	AB183859	Rabbit	1:1000	1:200
AKAP12	Sigma	HPA006344	Rabbit	1:1000	1:200
MT1	Abcam	AB12228	Mouse	1:1000	1:200
CRALBP	Abcam	AB1243664	Rabbit	N/A	1:500
Anti-rabbit-488	Invitrogen	A21206	Donkey	N/A	1:1000
Anti-mouse-594	Invitrogen	A21203	Donkey	N/A	1:1000
Hoechst 33342	Thermo Fisher	H3569	N/A	N/A	1μg/mL
Anti-rabbit IgG	Cell signalling	#7074	Goat	1:5000	N/A
Anti-mouse IgG	Cell signalling	#7076	Horse	1:5000	N/A

Declaration of interest

The authors declare that they have no conflict of interest.

Acknowledgement

All human eye tissues utilized in this research were sourced from the New South Wales Tissue Bank and provided through the Australian Ocular Biobank. This study received financial support from organizations including the Lowy Medical Research Institute (for MG, LZ and TZ), the National Health and Medical Research Council (Investigator Grant GNT_1195021 for MG, Idea grant GNT_2020950 for LZ), the Australian Vision Research (for MG, LZ and TZ) and the National Eye Institute (EY032462 and EY031324 for JD). The Innovation Team and Talents Cultivation Program of National Administration of TCM (ZYYCXTD-D-202002, X.F.), the Fundamental Research Funds for the Central Universities (226-2023-00114 and 226-2022-00226, X.F.). The authors thank the High-Performance Computing Cluster of Zhejiang University Innovation Centre of Yangtze River Delta for their technical support.

References

1. Zwanzig, A., et al., *Neuroprotective effects of glial mediators in interactions between retinal neurons and Muller cells.* Exp Eye Res, 2021. **209**: p. 108689.
2. Vecino, E., et al., *Glia-neuron interactions in the mammalian retina.* Prog Retin Eye Res, 2016. **51**: p. 1-40.
3. Fleckenstein, M., et al., *Age-related macular degeneration.* Nat Rev Dis Primers, 2021. **7**(1): p. 31.
4. Reichenbach, A. and A. Bringmann, *New functions of Muller cells.* Glia, 2013. **61**(5): p. 651-78.
5. Jorstad, N.L., et al., *Stimulation of functional neuronal regeneration from Muller glia in adult mice.* Nature, 2017. **548**(7665): p. 103-107.
6. Zhang, T., et al., *Human macular Muller cells rely more on serine biosynthesis to combat oxidative stress than those from the periphery.* Elife, 2019. **8**.
7. E, B.D. and G. Marfany, *The Relevance of Oxidative Stress in the Pathogenesis and Therapy of Retinal Dystrophies.* Antioxidants (Basel), 2020. **9**(4).
8. Bruera, M.G., et al., *Glial cell response to constant low light exposure in rat retina.* Vis Neurosci, 2022. **39**: p. E005.
9. Organisciak, D.T. and D.K. Vaughan, *Retinal light damage: mechanisms and protection.* Prog Retin Eye Res, 2010. **29**(2): p. 113-34.
10. Wenzel, A., et al., *Molecular mechanisms of light-induced photoreceptor apoptosis and neuroprotection for retinal degeneration.* Prog Retin Eye Res, 2005. **24**(2): p. 275-306.
11. Abbas, F., et al., *Revival of light signalling in the postmortem mouse and human retina.* Nature, 2022. **606**(7913): p. 351-357.
12. Yi, W., et al., *A single-cell transcriptome atlas of the aging human and macaque retina.* Natl Sci Rev, 2021. **8**(4): p. nwaa179.
13. Lenkowski, J.R. and P.A. Raymond, *Muller glia: Stem cells for generation and regeneration of retinal neurons in teleost fish.* Prog Retin Eye Res, 2014. **40**: p. 94-123.
14. Wolf, F.A., et al., *PAGA: graph abstraction reconciles clustering with trajectory inference through a topology preserving map of single cells.* Genome Biol, 2019. **20**(1): p. 59.
15. Pennesi, M.E., M. Neuringer, and R.J. Courtney, *Animal models of age related macular degeneration.* Mol Aspects Med, 2012. **33**(4): p. 487-509.
16. Albrecht, A.L., et al., *Basal and metal-induced expression of metallothionein isoform 1 and 2 genes in the RWPE-1 human prostate epithelial cell line.* J Appl Toxicol, 2008. **28**(3): p. 283-93.
17. Thakur, V., et al., *The membrane tethered matrix metalloproteinase MT1-MMP triggers an outside-in DNA damage response that impacts chemo- and radiotherapy responses of breast cancer.* Cancer Lett, 2019. **443**: p. 115-124.
18. Yang, L., et al., *Antioxidant metallothionein alleviates endoplasmic reticulum stress-induced myocardial apoptosis and contractile dysfunction.* Free Radical Research, 2015. **49**(10): p. 1187-1198.
19. Shimoda, R., et al., *Metallothionein is a potential negative regulator of apoptosis.* Toxicol Sci, 2003. **73**(2): p. 294-300.
20. Zareba, N. and M. Kepinska, *The Function of Transthyretin Complexes with Metallothionein in Alzheimer's Disease.* Int J Mol Sci, 2020. **21**(23).
21. Sharma, S.K. and M. Ebadi, *Metallothionein attenuates 3-morpholinosydnonimine (SIN-1)-induced oxidative stress in dopaminergic neurons.* Antioxid Redox Signal, 2003. **5**(3): p. 251-64.
22. Canto, A., et al., *Nitrosative Stress in Retinal Pathologies: Review.* Antioxidants (Basel), 2019. **8**(11).
23. Gelman, I.H., *The role of SSeCKS/gravin/AKAP12 scaffolding proteins in the spaciotemporal control of signaling pathways in oncogenesis and development.* Front Biosci, 2002. **7**: p. d1782-97.
24. Kwon, H.B., et al., *AKAP12 regulates vascular integrity in zebrafish.* Exp Mol Med, 2012. **44**(3): p. 225-35.
25. Lee, S.W., et al., *SSeCKS regulates angiogenesis and tight junction formation in blood-brain barrier.* Nat Med, 2003. **9**(7): p. 900-6.
26. Benz, P.M., et al., *AKAP12 deficiency impairs VEGF-induced endothelial cell migration and sprouting.* Acta Physiol (Oxf), 2020. **228**(1): p. e13325.

27. Seo, J.H., et al., *AKAP12 Supports Blood-Brain Barrier Integrity against Ischemic Stroke.* Int J Mol Sci, 2020. **21**(23).
28. Katsuoka, F. and M. Yamamoto, *Small Maf proteins (MafF, MafG, MafK): History, structure and function.* Gene, 2016. **586**(2): p. 197-205.
29. Deng, Y., et al., *The role and regulation of Maf proteins in cancer.* Biomark Res, 2023. **11**(1): p. 17.
30. Furuyama, K., et al., *Diabetes relief in mice by glucose-sensing insulin-secreting human α-cells.* Nature, 2019. **567**(7746): p. 43-48.
31. Gabrysova, L., et al., *Publisher Correction: c-Maf controls immune responses by regulating disease-specific gene networks and repressing IL-2 in CD4(+) T cells.* Nat Immunol, 2019. **20**(3): p. 374.
32. Tian, Y., et al., *Identification of diagnostic signatures associated with immune infiltration in Alzheimer's disease by integrating bioinformatic analysis and machine-learning strategies.* Front Aging Neurosci, 2022. **14**: p. 919614.
33. Wang, Q., et al., *Meta-Analysis of Parkinson's Disease and Alzheimer's Disease Revealed Commonly Impaired Pathways and Dysregulation of NRF2-Dependent Genes.* J Alzheimers Dis, 2017. **56**(4): p. 1525-1539.
34. Hetz, C., *The unfolded protein response: controlling cell fate decisions under ER stress and beyond.* Nat Rev Mol Cell Biol, 2012. **13**(2): p. 89-102.
35. Li, B., et al., *Metabolic Features of Mouse and Human Retinas: Rods versus Cones, Macula versus Periphery, Retina versus RPE.* iScience, 2020. **23**(11): p. 101672.
36. Gantner, M.L., et al., *Serine and Lipid Metabolism in Macular Disease and Peripheral Neuropathy.* N Engl J Med, 2019. **381**(15): p. 1422-1433.
37. Chen, Y., et al., *Isolation, Culture, and Identification of Primary Muller Cells from Human Retina.* Bio Protoc, 2021. **11**(19): p. e4179.
38. Butler, A., et al., *Integrating single-cell transcriptomic data across different conditions, technologies, and species.* Nat Biotechnol, 2018. **36**(5): p. 411-420.
39. McGinnis, C.S., L.M. Murrow, and Z.J. Gartner, *DoubletFinder: Doublet Detection in Single-Cell RNA Sequencing Data Using Artificial Nearest Neighbors.* Cell Syst, 2019. **8**(4): p. 329-337 e4.
40. Welch, J.D., et al., *Single-Cell Multi-omic Integration Compares and Contrasts Features of Brain Cell Identity.* Cell, 2019. **177**(7): p. 1873-1887 e17.
41. Jin, K., et al., *Single-Cell RNA Sequencing Reveals the Temporal Diversity and Dynamics of Cardiac Immunity after Myocardial Infarction.* Small Methods, 2022. **6**(3): p. e2100752.
42. Burkhardt, D.B., et al., *Quantifying the effect of experimental perturbations at single-cell resolution.* Nat Biotechnol, 2021. **39**(5): p. 619-629.
43. Bergen, V., et al., *Generalizing RNA velocity to transient cell states through dynamical modeling.* Nat Biotechnol, 2020. **38**(12): p. 1408-1414.
44. Boyle, E.I., et al., *GO::TermFinder--open source software for accessing Gene Ontology information and finding significantly enriched Gene Ontology terms associated with a list of genes.* Bioinformatics, 2004. **20**(18): p. 3710-5.